Earth and Planetary Science Letters 543 (2020) 116351

Contents lists available at ScienceDirect

Earth and Planetary Science Letters

www.elsevier.com/locate/epsl

Subduction initiation and the rise of the Shillong Plateau

Rishav Mallick [a,b,*], Judith A. Hubbard [a,b], Eric O. Lindsey [b], Kyle E. Bradley [a], James D.P. Moore [b], Aktarul Ahsan [c], A.K.M. Khorshed Alam [c], Emma M. Hill [a,b]

[a] Asian School of the Environment, Nanyang Technological University, Singapore
[b] Earth Observatory of Singapore, Nanyang Technological University, Singapore
[c] Geological Survey of Bangladesh, Dhaka, Bangladesh

ARTICLE INFO

Article history:
Received 3 October 2019
Received in revised form 13 May 2020
Accepted 15 May 2020
Available online xxxx
Editor: J.-P. Avouac

Keywords:
active tectonics
geodesy geology
mountain building
subduction initiation
Shillong Plateau
Surma Basin

ABSTRACT

Discrepancies between geodetically and geologically estimated thrust fault slip rates are generally viewed as a methodological problem. Even when slip rate is steady over geological time, a discrepancy may exist because each method is sensitive to different deformation processes. However, this offers a tool to estimate the partitioning of convergence between footwall and hanging wall deformation, and therefore a way to discriminate among orogenic styles. Here we investigate one such discrepancy for the Shillong Plateau, a basement-cored contractional orogen within the Himalayan foreland basin. Using a regional block model to explain the modern geodetic velocity field and explicit uncertainty analysis of the geologic rates, we show that this discrepancy cannot be reconciled simply by invoking uncertainties in individual methods.

Our results indicate that the Shillong Plateau is not an ongoing forward break of the Bhutan Himalayas, as was believed until recently. Instead, the observed inter-plate convergence and plateau uplift in this region may be driven primarily by an attempt of the negatively buoyant Indian passive margin lithosphere (the Surma Basin), south of the plateau, to initiate subduction. As a result, the uplift history of the plateau, which constrains the geologic rate, is significantly lower than expected given the geodetic convergence rate. We propose that this convergence is largely accommodated by the transport of the footwall into the mantle. This geodynamic scenario has important regional seismotectonic implications: (1) the cold and brittle sinking passive margin may have enabled the deep extent (~30 km) and therefore large magnitude of the M_W 8+ Shillong Earthquake of 1897; (2) the collapse of the Indian lithosphere into the mantle may have created the anomalously deep (~20 km) Surma Basin; and (3) this subsidence may also drive accelerated post-Miocene westward propagation of the Indo-Burman Wedge. We propose that the Shillong Plateau is the only modern example of passive margin collapse, and can serve as a natural laboratory to study the earliest phase of subduction.

1. Introduction

The past few decades have seen an increasing interest in comparing geodetically inferred short-term fault slip rates to geologic slip rates across convergent margins (Allmendinger et al., 2009; Avouac, 2015). Discrepancies in slip rate estimates have been explained by (1) time-varying fault slip rates, (2) systematic errors in the data (geologic and/or geodetic), (3) earthquake cycle effects and incomplete temporal sampling of modern rates, and/or (4) sensitivity of geodetic and geologic rates to different geodynamic processes.

In this paper, we are concerned with the last process. At convergent margins, slip on the plate boundary thrust results in (1) uplift of the hanging wall (due to *overthrusting*) and/or (2) transport of the footwall into the mantle in the form of subduction (*underthrusting*). In this situation, geologic slip rates derived from exhumation histories in the hanging wall (in the hinterland) represent the component of convergence that goes into overthrusting, and are insensitive to underthrusting. Modern interseismic geodetic velocity fields, on the other hand, record horizontal plate motions and the overall convergence between the hanging wall and footwall, but do not predict the partitioning between overthrusting and underthrusting. Therefore, a mismatch in rates from different time scales can carry information about the regional geodynamic processes at play.

* Corresponding author.
E-mail addresses: rishav001@e.ntu.edu.sg, mallickrishg@gmail.com (R. Mallick).

https://doi.org/10.1016/j.epsl.2020.116351

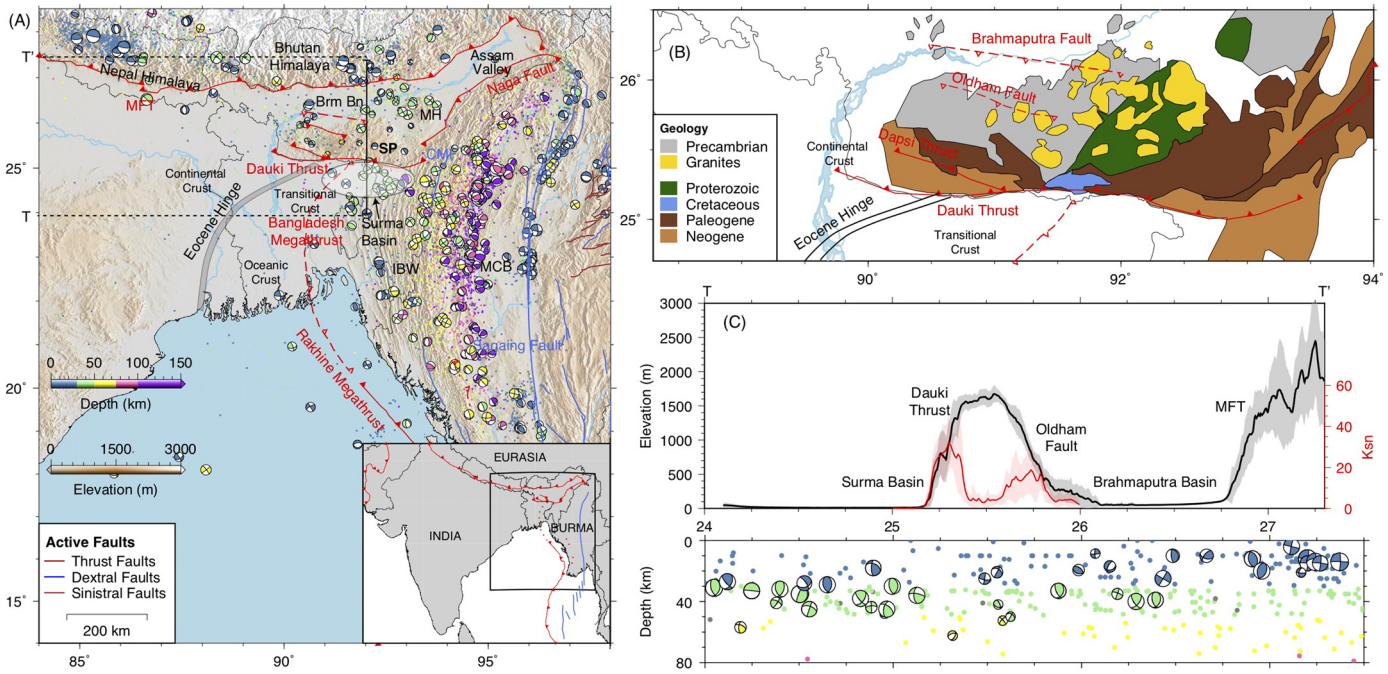

Fig. 1. Tectonic overview of the study area discussed in the paper. (A) Seismicity and focal mechanisms of earthquakes coloured by depth. Major plate boundaries and faults discussed in the paper are labelled. Inset map shows a zoomed out view of the India, Burma and Eurasia plates and plate boundaries. Brm Bn – Brahmaputra Basin, MFT – Main Frontal Thrust, SP – Shillong Plateau, MCB – Myanmar Central Basin, IBW – Indo-Burman Wedge, MH – Mikir Hills. (B) Lithologies in the Shillong Plateau; redrawn from Yin et al. (2010). We note the existence of crystalline basement outcrops within the Brahmaputra Basin. (C) The upper panel shows a topographic cross section (TT' in (A)) across the Shillong Plateau (black line with standard deviation in gray). The normalized river steepness (K_{SN}), calculated using TopoToolbox (Schwanghart and Scherler, 2014), is shown in red. High K_{SN} values are present near the Dauki Thrust and the Oldham Fault. The lower panel shows seismicity (dots) and focal mechanisms occurring within 100 km of TT', coloured by depth. Earthquakes south of the Shillong Plateau occur almost exclusively below 15 km, indicating brittle failure of the transitional-oceanic crust. (For interpretation of the colours in the figure(s), the reader is referred to the web version of this article.)

We investigate deformation associated with the Shillong Plateau, a ~1.5 km-high region of crystalline basement, deforming and growing in what should have been the Himalayan foreland basin, south of the Bhutan Himalaya (Fig. 1). The plateau is genetically a part of the Indian (continental) plate but appears to be deforming relative to stable India along the north-dipping Dauki Thrust (Fig. 1) as a new micro-plate (Bilham and England, 2001; Lindsey et al., 2018; Vernant et al., 2014). If the convergence here is accommodated by overthrusting, all of the accrued strain must result in topographic growth of the plateau. This has been the working hypothesis to describe the growth of the plateau (Bilham and England, 2001; Clark and Bilham, 2008).

This hypothesis has been tested with a combination of modern GPS shortening rates and long-term thermochronometry-derived cooling rates. The long-term shortening rate estimate of the plateau (0.5–2.5 mm/yr) comes from its uplift history recorded in the cooling ages of zircon and apatite grains since 8–14 Ma (Biswas et al., 2007; Clark and Bilham, 2008), while the modern GPS-derived convergence rates have a large range (2.5–9 mm/yr) owing to poor spatial and temporal data coverage (Bilham and England, 2001; Jade, 2004; Jade et al., 2007; Paul et al., 2001; Vernant et al., 2014). Some authors have suggested that the overlap in the ranges of estimated shortening rates from both methods (at least in part) implies that all of the convergence is transformed into plateau uplift, i.e. complete overthrusting. This has led to speculation that Shillong Plateau uplift is driven by a forward break of the Bhutan Himalaya, since the total India-Tibet shortening rate is higher here than to the west (Bilham and England, 2001; Clark and Bilham, 2008; Johnson and Nur Alam, 1991) (Fig. 2A).

In this study, we evaluate the statistical significance of the discrepancy in rates by updating the regional plate motion model for the Shillong Plateau and comparing the resulting 3-D velocity field to published geological and thermochronological results. We demonstrate that the difference in rates is statistically significant, which invalidates the hypothesis that overthrusting is the principal driver of this system. This implies that Shillong Plateau uplift is not driven by a forward break of the eastern Himalaya, but rather by a process that promotes underthrusting. The Surma Basin south of the Shillong Plateau is underlain by transitional-oceanic lithosphere, which is ideal for initiating subduction (Faccenna et al., 1999; Nikolaeva et al., 2010). We propose that the discrepancy in short-term and long-term rates can be explained by subduction initiation along the Dauki Thrust (Fig. 2B, C). This process would begin with subsidence of the crust south of the Shillong Plateau, which would pull the plateau to the south and generate convergence with limited topographic uplift. We discuss the implications of this process for regional tectonics and seismic hazards.

2. Data and methods

2.1. GPS data

We compiled GPS velocities from multiple sources in the ITRF08 reference frame (Barman et al., 2017; Jade et al., 2017; Kreemer et al., 2014; Mallick et al., 2019; Marechal et al., 2016; Vernant et al., 2014) and transformed these velocities to an India-stable reference frame using the Euler pole of Steckler et al. (2016). For datasets not in ITRF08 (Vernant et al., 2014), we first used a 6-parameter Helmert transformation to convert these velocities to ITRF08 using parameters for rotation and translation computed for sites common to the given dataset and Kreemer et al. (2014). While combining overlapping datasets we identified duplicate entries (less than 500 m apart) and computed a mean velocity and uncertainty (weighted by variance) to represent each of these stations. We used the uncertainties for the data as a weighting function, with a minimum threshold of 0.5 mm/yr to avoid overfitting. The final velocities in the India reference frame are available in Supplementary Table S1.

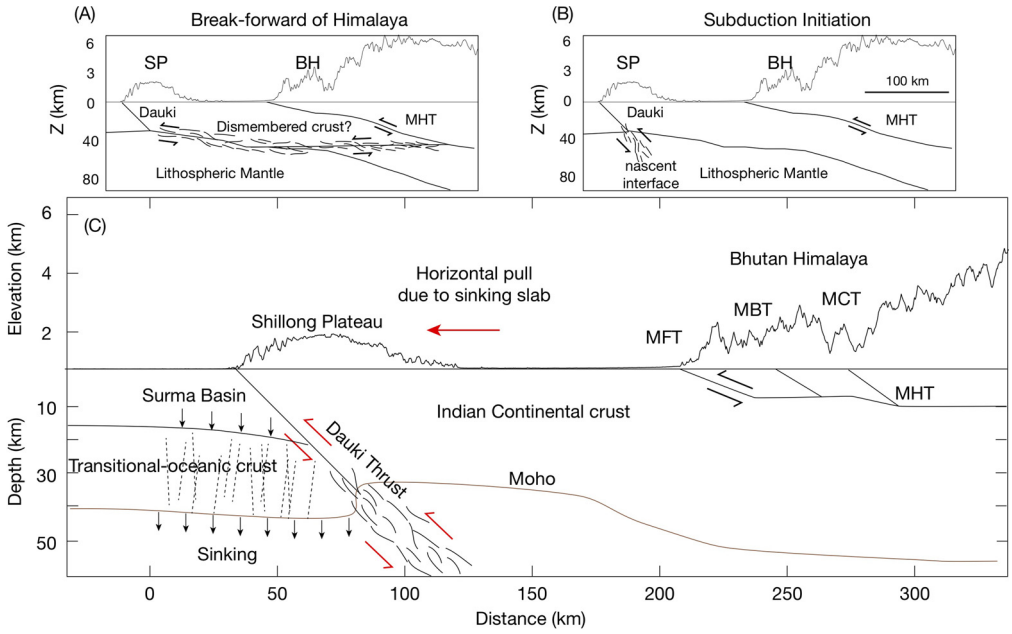

Fig. 2. Comparison of two candidate conceptual models that could be used to describe the tectonics of the Shillong Plateau. (A) The Main Himalayan Thrust (MHT) break forward hypothesis requires a 300 km connection between the deep decollement in the Bhutan Himalaya to the Dauki Thrust at ∼30 km depth. This will also imply dismemberment of the underthrusting Indian crust beneath the Himalayas. (B) Subduction Initiation of the Surma Basin along the pre-existent weak fabric of the Dauki Thrust due to the action of 15–20 km of sediment overburden and negatively buoyant transitional-oceanic crust. (C) Subduction Initiation model for the Surma Basin. We interpret the numerous near vertical fault plane solutions (dashed lines) for earthquakes within the transitional-oceanic crust (Fig. 1) as evidence of the mechanical resistance of the old rigid plate being overcome. SP – Shillong Plateau; BH – Bhutan Himalaya; MFT – Main Frontal Thrust; MBT – Main Boundary Thrust; MCT – Main Central Thrust.

2.2. Block modelling

We used the MATLAB-based Blocks software (Meade and Loveless, 2009) to model the GPS data $\boldsymbol{d}_{GPS}$. We assume that the GPS data represent a steady-state linear interseismic process, thereby allowing the multi-year timeseries to be described completely by a single value, velocity.

The velocity at any station is modeled as a sum of rigid plate/block rotations on a sphere and elastic strain accumulation on block boundaries (Meade and Loveless, 2009). We test for the residual post-seismic velocity field from the last great earthquake in the region, the 1897 M∼8 Shillong earthquake, and find that it may be safely neglected given commonly used parameter ranges for viscoelastic processes (Text S2; Figs. S3–S4).

We use 6 plates/blocks to model the GPS velocities: the Shillong Block (consisting of the Shillong Plateau, Mikir Hills, Brahmaputra Basin and Assam Valley), Indo-Burman Wedge, Myanmar Central Basin, Northern Shan Block, Shan Block and Indian plate/block (Fig. 3). We assume that some of these boundaries (Dauki Thrust, Rakhine-Bangladesh megathrust, Churachandpur-Mao Fault (CMF) and Sagaing Fault) are locked and accumulating strain at the full plate rate using a back-slip model to maintain continuity of the velocity field (Savage, 1983). In the following section, we briefly describe our block modelling method; for a detailed description we refer the reader to Text S1.

Each block can be described using its 3-component Euler vector, $\boldsymbol{\omega}$, which is linearly related to the GPS data for a given fault geometry, G_{GPS} (δ: dip; D: locking depth). In addition to GPS data, we also use a priori information on fault slip rates (G_{SR}) as a set of Gaussian constraint equations with unknown weights $\boldsymbol{d}_{SR} \sim N(\boldsymbol{\mu}_{SR}, \boldsymbol{\sigma}^2_{SR})$, specifically slip rate constraints on the CMF (assumed to be pure strike-slip) and the Dauki Thrust (assumed to be pure thrust) $(\overbrace{\sigma^2_{\mathrm{CMF}}, \sigma^2_{\mathrm{Dauki}}}^{\boldsymbol{\sigma}^2_{SR}})$.

$$\begin{bmatrix} \boldsymbol{d}_{GPS} \\ \boldsymbol{d}_{SR} \end{bmatrix} = \begin{bmatrix} G_{\mathrm{GPS}}(\delta, D) \\ G_{\mathrm{SR}}(\delta, D) \end{bmatrix} \boldsymbol{\omega} \tag{1}$$

Our goal is to find the range of values for $\boldsymbol{\omega}$, δ, D, $\boldsymbol{\sigma}^2_{SR}$ that can sufficiently explain the data given the priors. We do this using the combined covariance matrix (C_d) of the GPS data and slip rate priors as a way to weight the relative contribution of each dataset (Fukuda and Johnson, 2010).

$$C_d = \begin{bmatrix} C_d^{GPS} & 0 \\ 0 & C_d^{SR}(\boldsymbol{\sigma}^2_{SR}) \end{bmatrix} \tag{2}$$

We can write this as a problem in Bayesian parameter estimation, where we want to maximize the posterior probability density function (PDF) of the model parameters given the observed data, $p(\boldsymbol{\omega}, \delta, D, \boldsymbol{\sigma}^2_{SR} \mid \boldsymbol{d}_{GPS})$.

$$p\left(\boldsymbol{\omega}, \delta, D, \boldsymbol{\sigma}^2_{SR} \mid \boldsymbol{d}_{GPS}\right) = \frac{p(\boldsymbol{d}_{GPS} \mid \boldsymbol{\omega}, \delta, D, \boldsymbol{\sigma}^2_{SR}) p(\boldsymbol{\omega}, \delta, D, \boldsymbol{\sigma}^2_{SR})}{p(\boldsymbol{d}_{GPS})} \tag{3}$$

$p(\boldsymbol{d}_{GPS} \mid \boldsymbol{\omega}, \delta, D, \boldsymbol{\sigma}^2_{SR})$ is the data likelihood function, which we choose as a multivariate Gaussian distribution, while $p(\boldsymbol{\omega}, \delta, D, \boldsymbol{\sigma}^2_{SR})$ is the prior distribution on each of the model parameters. We assume uniform priors for $\boldsymbol{\omega}$, uniform positive priors for $\boldsymbol{\sigma}^2_{SR}$, and uniform priors in the interval $[0, 90]$ ° and $[0, 50]$ km for δ, D, respectively. We sample from Eq. (3) using a MATLAB-based slice sampler (Neal, 2003) to obtain a discrete representation of the posterior PDF of model parameters.

2.3. Uncertainties in long-term uplift rates

The geologic shortening rates for the Shillong Plateau come from estimates of long-term rock uplift rates that are converted to shortening through several assumptions (complete overthrusting, 2-d area balance, fixed detachment depth, etc.). In this paper, we deal directly with the thermochronological observables and derive

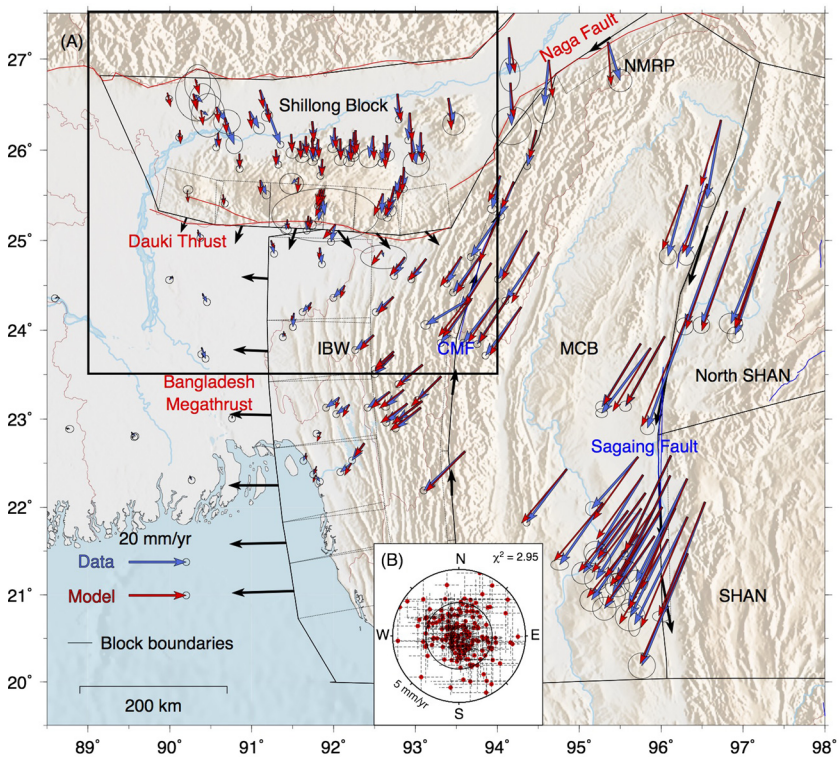

Fig. 3. (A) Data and model predicted velocities from our preferred block model (maximum posterior probability). Major block boundaries are labelled and coloured as in Fig. 1. The data (blue vectors), modelled velocities (red vectors) and block boundary slip rates (black vectors showing relative motion of the hanging wall) are all shown with the same scale. Station velocities are shown with their 95% confidence intervals as ellipses. Block names are labelled in black. Black box is the area shown in Fig. 4. (B) Residuals, shown as red circles in a polar plot with uncertainty as crosses, show no systematic spatial bias which indicates the model can satisfactorily explain the data (contours every 2.5 mm/yr; outer contour is 5 mm/yr). IBW – Indo-Burman Wedge; MCB – Myanmar Central Basin; CMF – Churachandpur-Mao Fault.

confidence bounds for the inferred uplift rates by propagating the uncertainties in each assumption through Monte-Carlo sampling.

Thermochronology studies have shown the rocks sampled within the Shillong Plateau, close to the Dauki Thrust, reset the U-Th-[Sm]/He apatite clock but not the U-Th/He zircon thermochron (Biswas et al., 2007; Clark and Bilham, 2008). Based on closure temperatures for apatite and zircon varying uniformly between [55, 85] °C and [170, 200] °C, respectively, and a geothermal gradient modeled as a truncated Gaussian distribution 30 ± 10 °C/km (truncated at 10 °C/km and 50 °C/km), we estimate the probability distribution of minimum and maximum Cenozoic sedimentary cover (Thickness $= \frac{T_{\text{closure}}}{\text{Geotherm}}$) initially deposited on the Shillong Plateau basement. From apatite dating, the initiation of rock uplift ($t_{\text{initiation}}$) is estimated between 8–14 Ma (Biswas et al., 2007; Clark and Bilham, 2008). The sedimentary cover was eroded away by 3–5 Ma to expose an erosion resistant crystalline basement which then began gaining elevation. The timing of this event (t_{topo}) is inferred from a change in sedimentary facies in the Surma Basin (Alam et al., 2003), the onset of flexural loading in the Surma Basin sediments (Najman et al., 2016), a volume balance of eroded material in catchments affected by the Dauki Thrust (Rosenkranz et al., 2018) and deflections in the paleodeposits of the Brahmaputra River as it moved north of the plateau due to the rising topography (Govin et al., 2018). If we assume that uplift was a steady linear process prior to exposure of the basement, we can use these constraints to stochastically estimate the Miocene rock uplift rate $\dot{U}_R^m$.

$$\dot{U}_R^m = \frac{\text{Thickness}}{t_{\text{initiation}} - t_{\text{topo}}} \tag{4}$$

The Pliocene-Present surface uplift rate $\dot{U}_S^p$ is estimated from the rate of elevation gain of a bevelled paleo surface cut into the basement rocks; its present elevation is 1500 ± 100 m and was thought to have been at sea level 3–5 Ma (Alam et al., 2003; Grujic et al., 2006). For the case of the paleo surface, the erosion rate $\dot{\epsilon} = 0$ because the surface is bevelled and smooth, indicating that it has been preserved since its last surface exposure in the Cretaceous (Alam et al., 2003). As a result, we can estimate the Pliocene rock uplift rate $\dot{U}_R^p$ from the topographic uplift rate and the erosion rate (England and Molnar, 1990).

$$\dot{U}_R^p = \dot{U}_S^p + \dot{\epsilon} \tag{5}$$

This surface appears to have been transported vertically with minimal tilting, meaning that rock uplift and erosion have acted uniformly on this plane; therefore Eq. (5) is applicable over the entire area.

3. Results

We show the results of our plate motion models for the Shillong Block, Indo-Burman Wedge, Myanmar Central Basin, Northern Shan Block and Shan Block relative to the Indian Plate/block (Fig. 3). Strain accumulation is assumed to have localized onto block boundary faults; their slip rates and orientations are shown as black arrows, while their geometries are shown as dashed lines. From the *maximum a posteriori* (MAP) block model, we estimate 30–35 mm/yr of oblique India-Shan convergence (azimuth ~40°); ~20 mm/yr of this north-south motion is accommodated by dextral strike-slip on the Sagaing Fault, while the rest (7–9 mm/yr) results in either localized dextral shear on the CMF and/or overall shear distributed among the megathrust and other faults within the Indo-Burman Wedge

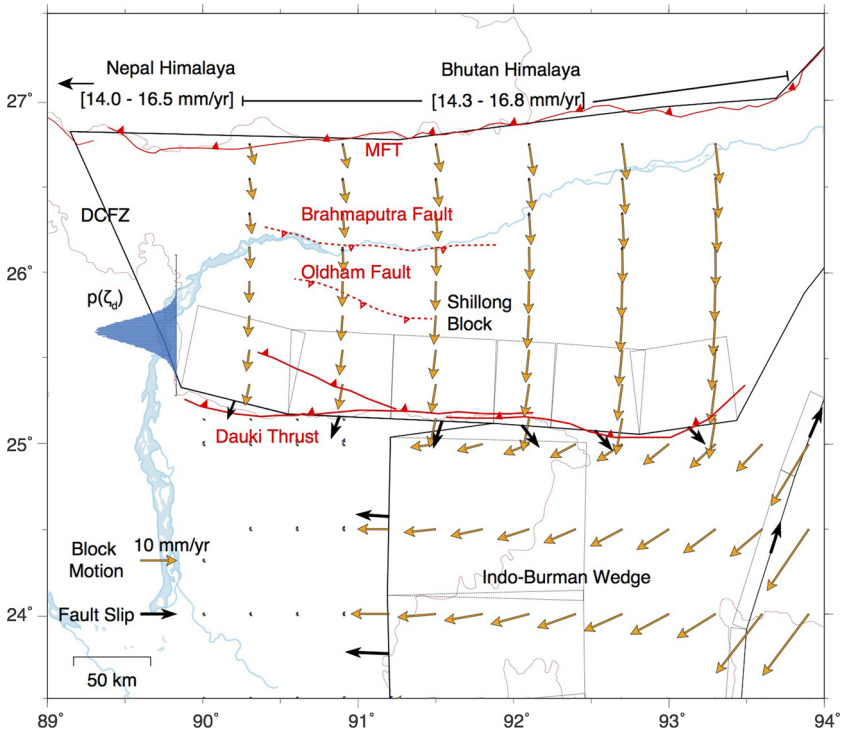

Fig. 4. Results of block modeling, focused on the Shillong Block area (black rectangle in Fig. 3). The orange vectors show the predicted long-term horizontal motion of the block relative to stable India. Inter-block slip rate vectors (motion of hanging wall relative to foot wall) are shown in black. The posterior PDF of the horizontal position of the locked-creeping transition in the Shillong Block is shown in blue as $p(\zeta_d)$. DCFZ indicates the Dhubri Chungthung Fault Zone while the major thrust faults are marked in red (dashed red lines are the inferred traces of the Oldham Fault and Brahmaputra Fault). The estimated slip rate for the Main Frontal Thrust (MFT) is from Lindsey et al. (2018).

(Mallick et al., 2019). The Rakhine-Bangladesh megathrust accommodates between 10–20 mm/yr of east-west convergence, with the magnitude increasing southwards. The Dauki thrust accommodates between 5–8 mm/yr of north-south convergence (Fig. 4), with a significant change in rake on either side of our chosen triple junction between the Indian Block, Indo-Burman Wedge and Shillong Block (Fig. 4, S2).

In the following sections we focus on the Shillong Block and discuss the detailed results of our study in two parts: (1) geometry and kinematics of the Shillong Block and (2) geometry and deformation associated with the Dauki Thrust.

3.1. Geometry and kinematics of the Shillong Block

We define the Shillong Block as the region encompassing the Shillong Plateau, Mikir Hills, Brahmaputra Basin and Assam Valley (Figs. 1, 3A), as this single block can sufficiently explain the geodetic velocity field (RMSE = 1.7 mm/yr; Fig. 3B). While a second block (Vernant et al., 2014) can improve the fit due to the addition of model parameters, the improvement is not statistically significant. For example, station NMRP in the Naga Hills is the easternmost point that we can use to constrain the rotation of the Shillong Block relative to the Myanmar Central Basin (Fig. 3A). We satisfactorily fit the station velocity (model velocity pierces the uncertainty ellipse), making it unnecessary to invoke additional blocks or block boundaries such as the Assam Block and Kopili Fault (Barman et al., 2017; Vernant et al., 2014) or the Badapani-Tryshad Shear Zone (Yin et al., 2010).

The northern boundary of the Shillong Block is defined by the Main Frontal Thrust (MFT) in Bhutan. While we do not model data from the Bhutan Himalaya in our block modelling framework, we note that in 2-D the velocity field across the MFT is continuous, indicating a locked shallow plate boundary (Fig. S7; also see Lindsey et al., 2018). Previous interpretations of shallow creep on the Bhutan MFT at a rate of ~5–7 mm/yr were based on station velocities resolved in an Indian plate reference frame but interpreted in a Shillong-fixed reference frame (Marechal et al., 2016). Here, we show that the Shillong Block has a coherent and finite southward velocity relative to India (Fig. 4), and thus shallow creep on the MFT is not necessary to explain the data (Fig. S7).

3.2. Dauki Thrust

We jointly infer the slip rate, geometry and weight of strike-slip penalization on the Dauki Thrust in our models (Figs. 3–4, S1–S2). The estimated fault slip rate increases from the west (~5 mm/yr) to the center (~7 mm/yr), and then decreases eastward (~6 mm/yr), indicating that the Shillong Block and Indo-Burman Wedge are co-rotating in a clockwise manner relative to the Indian plate (Fig. 5). We find that the depth and dip of the Dauki Thrust varies between $D \in [21, 37]$ (MAP = 27) km, $\delta \in [23, 40]$ (MAP = 28)° for our elastic block models (parameter ranges in brackets are 95% confidence intervals; Fig. S1). We note that the dip may represent an average dip for the system, i.e. if the Dauki Thrust flattens at depth as part of a ramp-flat system, our estimated dip is only a minimum value for the ramp. Thus, any predicted uplift rate (Slip rate $\times \sin\delta$) using this geometry is a minimum uplift rate.

The surface velocity field is most sensitive to the horizontal location of the locked-creeping transition of the block boundary $\zeta_d = \frac{D}{\tan\delta}$ (Lindsey et al., 2014; Mallick et al., 2019). Although the concept of a spatial step change in fault slip rate is unphysical, this is a common kinematic modelling simplification that exploits the fact that geodetic data cannot resolve the true transition width when using surface velocity gradients to infer fault slip rates at >20 km depth (Lindsey et al., 2014). We estimate ζ_d to be [30,55] km north of the trace of the Dauki Thrust (Fig. 4), close to the down-dip projection of the south-dipping blind Oldham and Brahmaputra Faults.

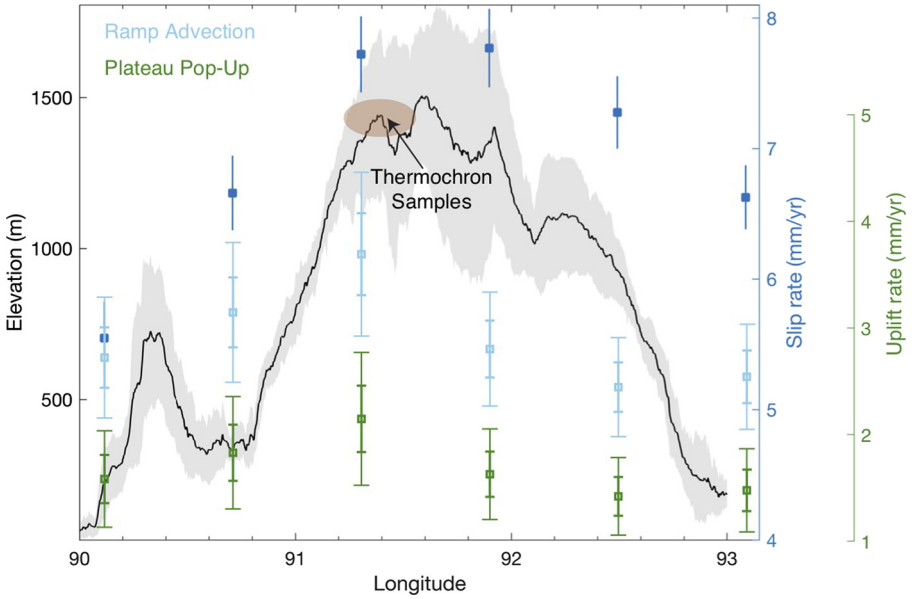

Fig. 5. Comparison of mean topography (black with standard deviation in gray) for a transect along the southern front of the Shillong Plateau, and predicted slip rate of the Dauki Thrust, in blue (with standard deviation). We also show the predicted (overthrusting) uplift rate for each of the rectangular Dauki Thrust segments in Fig. 4 calculated from two models: ramp advection (Slip rate $\times \sin\delta$) in light blue, and plateau pop-up ($\frac{\text{Slip rate}}{2} \times \tan\delta$) in green. For details, we refer the reader to Supplementary Section S4 and Fig. S6. The uplift rates are provided with ± 1 (bold error bar) and ± 2 (light error bar) standard deviations. All quantities increase from west to the center and then taper to the east.

Since the Dauki Thrust dips to the north while the Oldham and Brahmaputra Faults are thought to dip to the south (Bilham and England, 2001; Rajendran et al., 2004), it is likely that they would intersect close to our inferred locked-creeping transition and are part of the same system accumulating tectonic strain. Thus, even though we can estimate the rate of strain accumulation, we cannot distinguish between the Dauki Thrust or a combination of the Dauki Thrust and faults along the northern margin of the Shillong Plateau as the structures that will eventually accommodate this strain.

The estimated rake of the Dauki Thrust, which is a measure of the inter-block convergence obliquity, appears to vary from west to east along the fault. We explore the full range of penalizations of strike-slip motion on the Dauki Thrust (σ_{Dauki} in Fig. S1) and find that a variation in convergence obliquity from predominantly thrust (west of the triple junction in Fig. 4) to oblique with significant dextral motion (east of the triple junction), is necessary for our block models to fit the data. We posit that the dextral motion east of the triple junction may represent distributed shear within the Indo-Burman Wedge close to the Shillong Plateau rather than reflecting oblique slip on the Dauki fault itself (Text S3, Fig. S5).

4. Discussion

From our geodetic block model, we estimate the modern horizontal plate motions that drives the shortening of the Shillong Plateau. We explore if this horizontal convergence of 5–8 mm/yr (Fig. 5) is congruent with the geologic observables over the million-year timescale. Past studies relating short-term and long-term rates across plate boundary faults find that discrepancies in rates can often be attributed to methodological biases in both geological estimates (Donnellan et al., 1993) and geodetic models (Thompson et al., 2015). Viscoelastic relaxation of the mantle following earthquakes may also systematically lead to overestimates of modern rates (Perfettini and Avouac, 2004). In this study, we show that post-seismic relaxation effects are negligible (Fig. S3–S4). We formally quantify the uncertainties in the geologic and geodetic slip rate estimates to show that the discrepancies in slip rate estimates for the Dauki Thrust are statistically significant, and evaluate the seismotectonic implications.

4.1. Steady rock uplift?

Has rock uplift of the Shillong Plateau been steady through time? In order to assess this, we compare the probability distributions of the Miocene uplift rate $\dot{U}_R^m$ (Eq. (4)) and the Pliocene-present uplift rate $\dot{U}_S^p$ (Fig. 6). We find that the probability distributions overlap, and uplift could have been constant or decreased over time, but did not accelerate. We estimate the probability $p(\dot{U}_R^m > \dot{U}_R^p) = 80\%$ (Fig. 6B), indicating that the uplift rate likely decelerated from the Miocene to the Pliocene-present.

To compare the long term record with geodetic observations, we convert the estimated modern horizontal convergence rate (V_{pl}) to rock uplift at the locations where the thermochronological samples were obtained (Fig. 5) using two different overthrusting models. In Model 1, material advects upward along a δ-dipping ramp connected to a horizontal décollement, with a predicted uplift rate of 3.0–4.1 mm/yr (Fig. 5, 6B). In Model 2, long-term horizontal shortening is converted to uplift by rigid body transport of a trapezoidal plateau (details are in Text S4 and Fig. S6) bounded by oppositely dipping faults (Bilham and England, 2001), with a predicted uplift rate of 1.5–2.9 mm/yr (Fig. 5, 6B). There is insignificant (at the 99% confidence level) overlap of the probability distributions of the predicted modern uplift rate with either $\dot{U}_R^m$ or $\dot{U}_R^p$ (Fig. 6B), demonstrating that the discrepancy between the geologic and geodetic uplift rates is statistically significant. Reconciliation of these rates requires a process that produces lower uplift rates than either overthrusting model. A model that predicts a decrease in uplift rate over geological time would be preferred but not required, given the probability distributions that we calculate.

4.2. Evidence against break-forward of the Bhutan Himalaya

The break-forward model linking the Bhutan Himalaya to the Shillong Plateau has been the popular model of choice to describe the uplift of the plateau (Bilham and England, 2001;

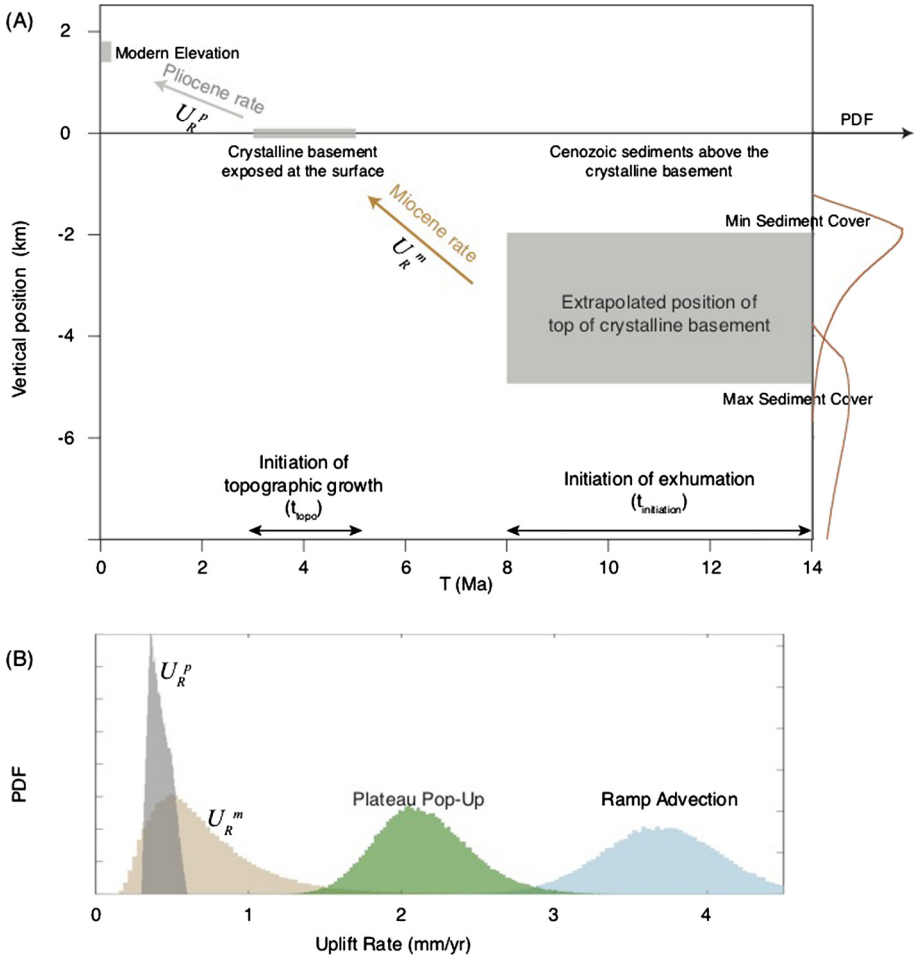

Fig. 6. Uplift history of the Shillong Plateau. (A) At 8–14 Ma, the top of the crystalline basement (gray rectangle does not carry any information on thickness of the basement) is at a depth of 2–5 km. The probability distribution functions (PDF) of the minimum and maximum depth of the top of the crystalline basement, which are actually estimates of the sedimentary overburden are shown as brown lines. This sedimentary overburden is removed from $t_{\text{initiation}}$ to t_{topo} at $\dot{U}_R^m$ mm/yr. Subsequently the plateau gained topography at $\dot{U}_R^p$ mm/yr. (B) Probability distribution of uplift rates in the Miocene (brown) vs. Pliocene-present (gray) from propagation of uncertainties in sedimentary thickness and timing information ($t_{\text{initiation}}$ and t_{topo}). Rock uplift rates predicted from the modern convergence rate assuming complete overthrusting are shown for two different uplift mechanisms: blue (ramp advection) and green (pop-up). There is almost no overlap between the modern uplift rate PDFs and either geological uplift rate PDF, indicating that shortening must be in part accommodated by underthrusting.

Clark and Bilham, 2008; Johnson and Nur Alam, 1991). It combines an assumption of *complete overthrusting* with the observation that the southward components of the velocities (in an Indian reference frame) show a west to east increase in southern Tibet, rising from 15 to 20 mm/yr (Lindsey et al., 2018; Vernant et al., 2014). Superficially, it looks like the increased convergence is partitioned between the Main Himalayan Thrust (MHT) and the Dauki Thrust; these faults are assumed to be somehow linked by a (sub) horizontal detachment (Fig. 2A) or by transmission of collisional in-plane stresses into the foreland (Bilham and England, 2001). This model implies that over multiple earthquake cycles, the Indian plate is stationary, and all inter-block convergence is accommodated by thrusting of the Shillong Plateau over the Surma Basin along the Dauki Thrust, either as a crustal scale fault-propagation fold (Clark and Bilham, 2008), or as a pop-up structure (Bilham and England, 2001).

The exhumation history demonstrates that some overthrusting has occurred. This is consistent with the Bouguer gravity anomaly over the Shillong Plateau, which is positive (∼50 mGal), indicating uncompensated topography (i.e. a lack of crustal root to support the ∼1.5 km topography) (Nayak et al., 2008). Joint inversions of receiver functions and surface wave dispersion do not show thickened crust supporting the Shillong Plateau (Mitra et al., 2018; Priestley et al., 2019). This lack of a crustal root implies that the plateau is being thrust on top of the Indian plate and is held up by the elastic strength of the lithosphere (Lyon-Caen and Molnar, 1985). However, these observations do not imply break-forward of the Bhutan Himalaya due to the following reasons:

(1) The long-term uplift rates are significantly lower than what we predict from the modern convergence rate (Text S4, Figs. 6, S6), implying that overthrusting is only a minor component of the convergence. The only overthrusting model that can match the geological uplift rates is one where the Shillong Plateau deforms in isostatically balanced pure shear (Text S4, Fig. S6). However, this model requires the existence of a crustal root, which is not seen in geophysical observations of the Moho (Mitra et al., 2018; Priestley et al., 2019).

(2) The Moho beneath the plateau is ∼35 km deep (Mitra et al., 2018), while the MHT is only 10–20 km deep (Coutand et al., 2014); connecting these systems would require dismembering the Indian lower crust underthrusting Tibet (Fig. 2A). An alternative model of plateau pop-up resulting from in-plane compression does not require a physical connection between the MHT and the Shillong Plateau (Bilham and England, 2001). However, the predicted geological uplift rate from this model is still significantly greater (at the 99% confidence level) than the observed rates (Fig. 6, S6).

(3) Uplift of the Shillong Plateau has been synchronous with the development of the Main Central Thrust (MCT), Main Boundary Thrust (MBT) and Main Frontal Thrust (MFT) in the Himalaya. Given the amount of shortening that has accumulated on these faults and the overall southward propagation of the MHT (Avouac, 2015), the Himalayan deformation front would likely have been greater than 400 km further north from the Dauki Thrust in the Miocene than it is today, making it that much harder to physically link these systems.

Together, these points demonstrate that kinematic linkage between the Himalaya and the Shillong Plateau through breakforward is implausible.

4.3. Subduction initiation of Transitional-Oceanic Indian lithosphere

We propose that subduction initiation of the lithosphere underlying the Surma Basin can explain the mismatch in long-term uplift rates compared to modern shortening rates. Subduction initiation at passive margins is difficult to achieve due to the rigidity and bending resistance of old lithosphere (Gregg Erickson, 1993; Mueller and Phillips, 1991), and passive margin subduction initiation has not thus far been identified in the Cenozoic (Stern, 2004). However, the crust underlying the ~15 km sedimentary pile of the Surma Basin displays a number of characteristics that prompt us to suggest that it may indeed have overcome any resistive forces and is attempting to subduct.

The crust beneath the Surma Basin is thought to have formed in the Cretaceous (~130 Ma), when India-Antarctica rifting began (Alam et al., 2003; Johnson and Nur Alam, 1991). Although this rift zone is now buried under sediments, its signal remains as a Bouger gravity anomaly high around the paleo margin/hinge, which separates oceanic crust to the east from Precambrian continental crust to the west (Mitra et al., 2018; Talwani et al., 2016) (labelled as the Hinge Zone in Fig. 1A). East of the hinge zone and beneath the ~15 km pile of sediments in the Surma Basin is a volcanic rifted margin; this was created by magmatic intrusion of basaltic material within the stretched and thinned continental crust (Menzies et al., 2002). Hot spot volcanism from the Kerguelen plume, which postdates the initial rifting by 5–10 Ma, may have further densified and simultaneously weakened the crust during eruptive episodes such as those that produced the Sylhet Traps (Alam et al., 2003; Talwani et al., 2016). Modern observations of crustal structure in this region show that the Surma Basin crust has a thickness of 15-20 km and shear wave velocity ~4 km/s, both of which are significantly different from values expected for continental or oceanic crust, and hence it is called *transitional-oceanic crust* (Mitra et al., 2018) (Fig. 7). We take these observations to imply that the transitional-oceanic crust beneath the Surma Basin is negatively buoyant and can subduct.

Moderate sized earthquakes along steeply dipping faults, oriented approximately parallel to the hinge zone, systematically break the transitional-oceanic crust (Kumar et al., 2015; Mitra et al., 2018) (Fig. 1A, C). This seismicity may represent reactivation of crustal weaknesses along inherited structure (Kumar et al., 2015; Talwani et al., 2016) as the Indian slab tries to collapse into the mantle. These earthquakes are almost exclusive to the basement (not the sediment pile) (Fig. 1C), and may be assisted by fluids in the lower crust and lithosphere (Regenauer-Lieb et al., 2001), as active crustal faulting can create conduits for fluids to permeate to greater depths and enable aqueous metamorphic transformations (Jamtveit et al., 2018). Such metamorphic transformations are crucial in the ensuing stress balance, which determines whether the resisting forces present in an old, cold, and rigid lithosphere of a passive margin can be overcome by buoyancy or if the subduction zone freezes (Nikolaeva et al., 2010; Regenauer-Lieb et al., 2001).

Receiver functions image a deepening of the Moho from ~35 km at a station positioned directly above the Dauki Thrust, to ~50 km at a site within the Surma Basin (Mitra et al., 2018) (Fig. 7), which suggests that the Dauki Thrust may have already facilitated at least 15 km of transport of the Indian transitional-oceanic crust into the mantle.

Together, the geologic history of the Indian transitional-oceanic crust, active faulting along pre-existing weak zones in the crust and deepening of the Moho, serves as evidence for the collapse of a passive margin due to a buoyancy instability that could eventually result in the creation of a new subduction zone (Nikolaeva et al., 2010). Thus, the Surma Basin may be the first Cenozoic example of subduction initiation at a passive margin (Fig. 7). However, given the three-dimensional aspect of the crustal geometry, it is unclear if this subduction initiation is spontaneous or whether it partially results from momentum transfer from the nearby active subduction of the Indian plate beneath the Burma plate (Mallick et al., 2019; Steckler et al., 2016).

Analog and numerical experiments suggest that as a negatively buoyant slab initiates the process of sinking into the mantle, it will pull the continental upper plate towards itself, leading to horizontal convergence and overthrusting (Fig. 2C; Nikolaeva et al., 2010). In our study area, this initial convergence would promote overthrusting of the Shillong Plateau, as observed for the Miocene (Fig. 6). Experiments further indicate that if the convergent margin were to evolve into a self-sustained subduction zone, this overthrusting would slow down while horizontal shortening and basin subsidence would continue (Faccenna et al., 1999; Gurnis, 1992). In our case, this is consistent with the possible decrease in the Pliocene uplift rate of the plateau (Fig. 6) and the continued subsidence of the Surma Basin. This implies that the horizontal convergence across the Dauki Thrust has been mostly accommodated by significant footwall transport into the mantle (Fig. 7). This mechanism may also explain the increased India-Tibet modern GPS-velocities in the eastern Himalaya (compared to neighbouring Nepal) if the horizontal pull generated by the sinking transitional-oceanic plate is transmitted through the Indian continental lithosphere in a rigid manner (i.e. without stretching it like in a back-arc setting) (Fig. 2C).

The process of sinking of the Surma Basin due to subduction initiation can explain its great depth (>15 km) (Alam et al., 2003; Johnson and Nur Alam, 1991; Najman et al., 2016). This basin is typically explained as being flexurally loaded by the topography of the Shillong Plateau (Johnson and Nur Alam, 1991). However, the Surma Basin is significantly deeper than the 3–8 km foredeep of the Himalaya (Lyon-Caen and Molnar, 1985; Mitra et al., 2018). Given that the Himalaya are on average three times taller than the Shillong Plateau, this implies that the subsidence is in excess of what is expected from topographic loading by the nearby orogen. However, excess subsidence is expected if the Surma Basin is sinking into the mantle. This also has implications for the Indo-Burman Wedge (Fig. 7): the high mass storage ability of the Surma Basin may affect the growth and propagation of the outer Indo-Burman wedge by flexurally increasing its topographic slope. As sinking perturbs the wedge from its critical taper, it is forced to propagate westwards to reduce its taper and equilibrate. The long-term record appears consistent with this, showing at least 38 km of arc-perpendicular shortening over the past 8 Ma with an accelerated westward propagation of the deformation front in the Late Miocene (Betka et al., 2018).

4.4. Seismic hazard implications for the Shillong Plateau

A cold, sinking slab depresses the geotherm, which should promote brittle behaviour to greater depths along the nascent subduction interface (Syracuse et al., 2010). This could explain the 21–37

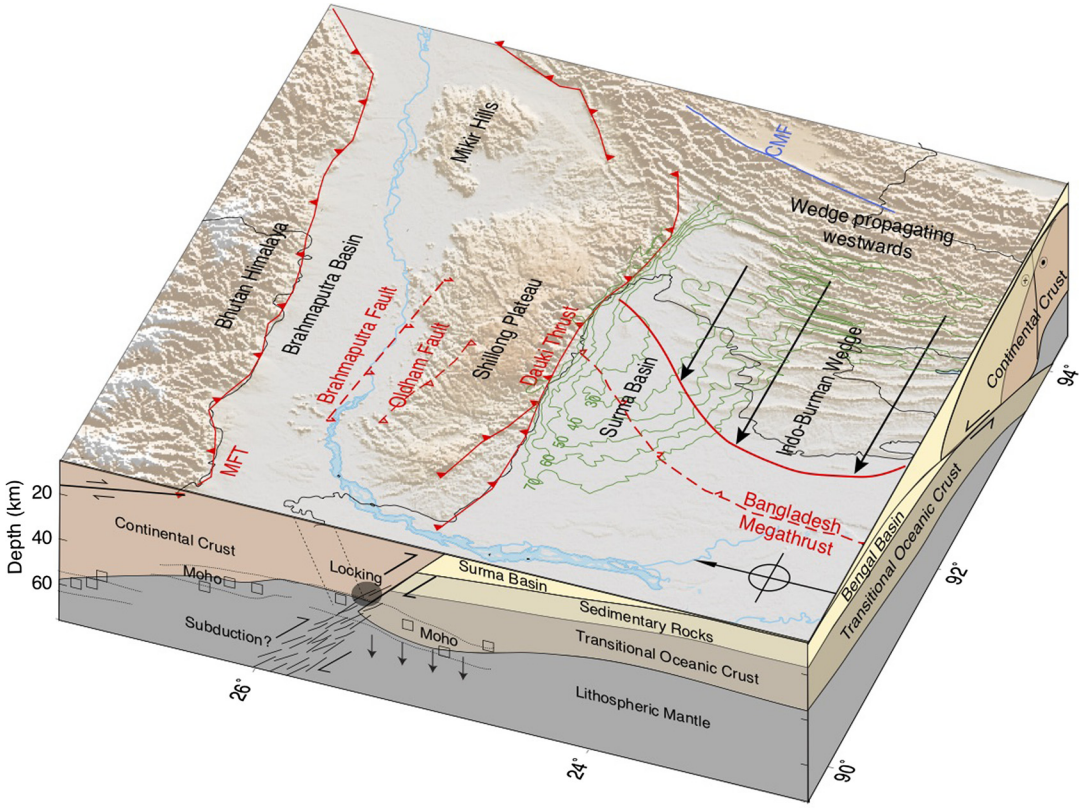

Fig. 7. Perspective view of the study area discussed in this paper. The Surma Basin (delineated by Bouguer anomaly contours (mGal) in green) is a passive margin that has been transformed to an active margin by possibly initiating a buoyancy instability in the Miocene. This has promoted some overthrusting of the Shillong massif, allowing it to build up ∼1.5 km of topography. The Moho in the cross-sectional view is inferred from seismological investigations of crustal structure (dotted regions – receiver functions; black boxes – surface wave dispersion; Mitra et al., 2018; Priestley et al., 2019). The collapse of the Surma Basin into the mantle as well as the rigid Shillong Plateau affect the westward propagation of the Indo-Burman Wedge. We show the edge of the outer fold belt as a red continuous line, and the blind fold belt as a dashed line (Bangladesh megathrust). The cross-sectional view of crustal structure beneath the Indo-Burman Wedge is redrawn from Wang et al. (2019).

km locking depth of the Dauki Thrust (Fig. 7), which is deeper than the typical brittle-ductile transition depth of 10–15 km observed in continental fold-thrust belts. This extended seismogenic thickness should permit earthquake ruptures to reach greater depths. This may explain the unusual dimensions of the M∼8+ 1897 Great Shillong Earthquake (100 km along strike, reaching 30 km depth, up to 25 m slip) (Bilham and England, 2001; England and Bilham, 2015).

From our geodetic block model, we estimate a moment accumulation rate of $\dot{M}_0 = 1.4\text{–}2.1 \times 10^{18}$ N-m/yr (potency rate for the Shillong Plateau $= 48\text{–}71 \times 10^6$ m^3/yr), comparable to previous estimates (England and Bilham, 2015). This accumulated elastic strain must be released in earthquakes and/or post-seismic processes along active faults (Dapsi Thrust, Dauki Thrust, Oldham Fault, Brahmaputra Fault, and Chedrang Fault). In the 122 years since the last great earthquake in this region, strain equivalent to a M_W 7.3–7.6 earthquake has already accrued within the Shillong Plateau. This represents a significant seismic hazard and risk to the populations of eastern India, Bangladesh and western Myanmar and yet it is only the minimum hazard estimate, since we assumed the 1897 event fully relaxed the crust. However, when we consider the ∼300 km length of the Dauki Thrust, together with the Dapsi Thrust has not ruptured in at least the last 500 years, if not longer (Rajendran et al., 2004; Steckler et al., 2008), the accumulated strain reservoir grows almost by an order of magnitude.

5. Conclusions

Sinking of the negatively buoyant transitional-oceanic lithosphere below the Surma basin may represent the only Cenozoic example of passive margin subduction initiation. This process likely began 8–14 Ma. In a first stage, slip on the Dauki Thrust caused by sinking of the footwall pulled the Shillong Plateau to the south and caused it to rise; erosion kept pace with uplift, ensuring no topography was built. In a second stage, once the Cretaceous sedimentary package was eroded away, the decreased erodibility of the exposed crystalline basement of the plateau allowed it to gain elevation. In the present day, the horizontal pull generated by this sinking of the Indian plate south of the Shillong Plateau must be dragging the Indian continental lithosphere southwards and leading to the increased geodetic convergence rate between India and the Bhutan Himalaya, compared to the neighbouring Nepal Himalaya. The collapsing Surma Basin may also affect the propagation of the Indo-Burman Wedge, and may be the cause of a documented acceleration in westward propagation of the wedge since the Miocene. The cold and brittle nature of the transitional-oceanic Indian lithosphere widens the seismogenic zone, presenting an increased seismic risk to the people of India, Bangladesh and Myanmar.

Declaration of competing interest

The authors declare that they have no known competing financial interests or personal relationships that could have appeared to influence the work reported in this paper.

Acknowledgements

All figures in this paper were made using MATLAB and Generic Mapping Tools (http://doi.wiley.com/10.1029/98EO00426). The GPS

velocities are provided as a text file in the supplementary materials. The code used in this paper and model outputs are available at (https://researchdata.ntu.edu.sg/dataverse/shillongmibb). The MATLAB based software Blocks is available here (https://github.com/jploveless/Blocks). TopoToolbox (available at https://github.com/wschwanghart/topotoolbox) was used to calculate the stream steepness indices in Fig. 1C. Seismicity and focal mechanisms were taken from GCMT (www.globalcmt.org, doi:10.1016/j.pepi.2012.04.002), ISC (https://doi.org/10.31905/D808B830) and (Kayal et al., 2012; Kumar et al., 2015). This research was supported by the Earth Observatory of Singapore and the National Research Foundation Singapore and the Singapore Ministry of Education under the Research Centres of Excellence initiative, and by a Singapore National Research Foundation Investigatorship awarded to EMH (Proposal ID NRF2018NRF-NRFI001-21). The authors are grateful for constructive reviews and suggestions by the Editor Jean-Philippe Avouac, Magali Billen, Jack Loveless and an anonymous reviewer. RM would like to thank the organizers of the field trip (Dave Lageson, Devon Orme, Mary Hubbard) run during HKT 2019, which helped him to understand the geology of a basement-cored uplift; and Pavel Adamek for linguistic advice. This is EOS paper number 298.

Appendix A. Supplementary material

Supplementary material related to this article can be found online at https://doi.org/10.1016/j.epsl.2020.116351.

References

Alam, M., Alam, M.M., Curray, J.R., Chowdhury, M.L.R., Gani, M.R., 2003. An overview of the sedimentary geology of the Bengal Basin in relation to the regional tectonic framework and basin-fill history. Sediment. Geol. 155, 179–208. https://doi.org/10.1016/S0037-0738(02)00180-X.

Allmendinger, R.W., Loveless, J.P., Pritchard, M.E., Meade, B., 2009. From decades to epochs: spanning the gap between geodesy and structural geology of active mountain belts. J. Struct. Geol. 31, 1409–1422. https://doi.org/10.1016/j.jsg.2009.08.008.

Avouac, J.P., 2015. Mountain building: from earthquakes to geologic deformation. In: Treatise on Geophysics. Elsevier, pp. 381–432.

Barman, P., Jade, S., Shrungeshwara, T.S., Kumar, A., Bhattacharyya, S., Ray, J.D., Jagannathan, S., Jamir, W.M., 2017. Crustal deformation rates in Assam Valley, Shillong Plateau, Eastern Himalaya, and Indo-Burmese region from 11 years (2002–2013) of GPS measurements. Int. J. Earth Sci. 106, 2025–2038. https://doi.org/10.1007/s00531-016-1407-z.

Betka, P.M., Seeber, L., Thomson, S.N., Steckler, M.S., Sincavage, R., Zoramthara, C., 2018. Slip-partitioning above a shallow, weak décollement beneath the Indo-Burman accretionary prism. Earth Planet. Sci. Lett. 503, 17–28. https://doi.org/10.1016/j.epsl.2018.09.003.

Bilham, R., England, P., 2001. Plateau "pop-up" in the great 1897 Assam earthquake. Nature 410, 806–809. https://doi.org/10.1038/35071057.

Biswas, S., Coutand, I., Grujic, D., Hager, C., Stöckli, D., Grasemann, B., 2007. Exhumation and uplift of the Shillong Plateau and its influence on the eastern Himalayas: new constraints from apatite and zircon (U-Th-[Sm])/He and apatite fission track analyses. Tectonics 26. https://doi.org/10.1029/2007TC002125.

Clark, M.K., Bilham, R., 2008. Miocene rise of the Shillong Plateau and the beginning of the end for the Eastern Himalaya. Earth Planet. Sci. Lett. 269, 336–350. https://doi.org/10.1016/j.epsl.2008.01.045.

Coutand, I., Whipp, D.M., Grujic, D., Bernet, M., Fellin, M.G., Bookhagen, B., Landry, K.R., Ghalley, S.K., Duncan, C., 2014. Geometry and kinematics of the Main Himalayan Thrust and Neogene crustal exhumation in the Bhutanese Himalaya derived from inversion of multithermochronologic data. J. Geophys. Res., Solid Earth 119, 1446–1481. https://doi.org/10.1002/2013JB010891.

Donnellan, A., Hager, B.H., King, R.W., 1993. Discrepancy between geological and geodetic deformation rates in the Ventura basin. Nature 366, 333–336. https://doi.org/10.1038/366333a0.

England, P., Bilham, R., 2015. The Shillong Plateau and the great 1897 Assam earthquake. Tectonics, 1792–1812. https://doi.org/10.1002/2015TC003902. Received.

England, P., Molnar, P., 1990. Surface uplift, uplift of rocks, and exhumation of rocks. Geology 18, 1173–1177. https://doi.org/10.1130/0091-7613(1990)018<1173:SUUORA>2.3.CO;2.

Faccenna, C., Giardini, D., Davy, P., Argentieri, A., 1999. Initiation of subduction at Atlantic-type margins: insights from laboratory experiments. J. Geophys. Res., Solid Earth 104, 2749–2766. https://doi.org/10.1029/1998JB900072.

Fukuda, J., Johnson, K.M., 2010. Mixed linear-non-linear inversion of crustal deformation data: Bayesian inference of model, weighting and regularization parameters. Geophys. J. Int. 181, 1441–1458. https://doi.org/10.1111/j.1365-246X.2010.04564.x.

Govin, G., Najman, Y., Copley, A., Millar, I., van der Beek, P., Huyghe, P., Grujic, D., Davenport, J., 2018. Timing and mechanism of the rise of the Shillong Plateau in the Himalayan foreland. Geology 46, 279–282. https://doi.org/10.1130/G39864.1.

Gregg Erickson, S., 1993. Sedimentary loading, lithospheric flexure, and subduction initiation at passive margins. Geology 21, 125–128. https://doi.org/10.1130/0091-7613(1993)021<0125:SLLFAS>2.3.CO;2.

Grujic, D., Coutand, I., Bookhagen, B., Bonnet, S., Blythe, A., Duncan, C., 2006. Climatic forcing of erosion, landscape, and tectonics in the Bhutan Himalayas. Geology 34, 801–804. https://doi.org/10.1130/G22648.1.

Gurnis, M., 1992. Rapid continental subsidence following the initiation and evolution of subduction. Science 80 (255), 1556–1558. https://doi.org/10.1126/science.255.5051.1556.

Jade, S., 2004. Estimates of plate velocity and crustal deformation in the Indian subcontinent using GPS geodesy. Curr. Sci.

Jade, S., Mukul, M., Bhattacharyya, A.K., Vijayan, M.S.M., Jaganathan, S., Kumar, Ashok, Tiwari, R.P., 2007. Estimates of interseismic deformation in Northeast India from GPS measurements. Earth Planet. Sci. Lett. 263, 221–234. https://doi.org/10.1016/j.epsl.2007.08.031.

Jade, S., Shrungeshwara, T.S., Kumar, K., Choudhury, P., Dumka, R.K., Bhu, H., 2017. India plate angular velocity and contemporary deformation rates from continuous GPS measurements from 1996 to 2015. Sci. Rep. 7, 11439. https://doi.org/10.1038/s41598-017-11697-w.

Jamtveit, B., Ben-Zion, Y., Renard, F., Austrheim, H., 2018. Earthquake-induced transformation of the lower crust. Nature 556, 487–491. https://doi.org/10.1038/s41586-018-0045-y.

Johnson, S.Y., Nur Alam, A.M., 1991. Sedimentation and tectonics of the Sylhet trough, Bangladesh. Geol. Soc. Am. Bull. https://doi.org/10.1130/0016-7606(1991)103<1513:SATOTS>2.3.CO;2.

Kayal, J.R., Arefiev, S.S., Baruah, Saurabh, Hazarika, D., 2012. Large and great earthquakes in the Shillong Plateau-Assam valley area of Northeast India region: pop-up and transverse tectonics. Tectonophysics 532–535, 186–192. https://doi.org/10.1016/j.tecto.2012.02.007.

Kreemer, C., Klein, E., Shen, Z.-K., Wang, M., Estey, L., Wier, S., Boler, F., 2014. A geodetic platemotion and global strain rate model. Geochem. Geophys. Geosyst. 130. https://doi.org/10.1002/2014GC005407.Received.

Kumar, A., Mitra, S., Suresh, G., 2015. Seismotectonics of the eastern Himalayan and Indo-Burman plate boundary systems. Tectonics 34, 2279–2295. https://doi.org/10.1002/2015TC003979.

Lindsey, E.O., Almeida, R., Mallick, R., Hubbard, J., Bradley, K., Tsang, L.L.H., Liu, Y., Burgmann, R., Hill, E.M., 2018. Structural control on down-dip locking extent of the Himalayan megathrust. J. Geophys. Res., Solid Earth, 1–14. https://doi.org/10.1029/2018JB015868.

Lindsey, E.O., Sahakian, V.J., Fialko, Y., Bock, Y., Barbot, S., Rockwell, T.K., 2014. Interseismic strain localization in the San Jacinto fault zone. Pure Appl. Geophys. 171, 2937–2954. https://doi.org/10.1007/s00024-013-0753-z.

Lyon-Caen, H., Molnar, P., 1985. Gravity anomalies, flexure of the Indian Plate, and the structure, support and evolution of the Himalaya and Ganga Basin. Tectonics 4, 513–538.

Mallick, R., Lindsey, E.O., Feng, L., Hubbard, J., Banerjee, P., Hill, E.M., 2019. Active convergence of the India-Burma-Sunda plates revealed by a new continuous GPS network. J. Geophys. Res., Solid Earth 124, 3155–3171. https://doi.org/10.1029/2018JB016480.

Marechal, A., Mazzotti, S., Cattin, R., Cazes, G., Vernant, P., Drukpa, D., Thinley, K., Tarayoun, A., Le Roux-Mallouf, R., Thapa, B.B., Pelgay, P., Gyeltshen, J., Doerflinger, E., Gautier, S., 2016. Evidence of interseismic coupling variations along the Bhutan Himalayan arc from new GPS data. Geophys. Res. Lett. 43, 12,399–12,406. https://doi.org/10.1002/2016GL071163.

Meade, B.J., Loveless, J.P., 2009. Block modeling with connected fault-network geometries and a linear elastic coupling estimator in spherical coordinates. Bull. Seismol. Soc. Am. 99, 3124–3139. https://doi.org/10.1785/0120090088.

Menzies, M.A., Klemperer, S.L., Ebinger, C.J., Baker, J., 2002. In: Volcanic Rifted Margin Characteristics, pp. 1–14.

Mitra, S., Priestley, K.F., Borah, K., Gaur, V.K., 2018. Crustal structure and evolution of the Eastern Himalayan Plate boundary system, Northeast India. J. Geophys. Res., Solid Earth 123, 621–640. https://doi.org/10.1002/2017JB014714.

Mueller, S., Phillips, R.J., 1991. On the initiation of subduction. J. Geophys. Res. 96, 651. https://doi.org/10.1029/90JB02237.

Najman, Y., Bracciali, L., Parrish, R.R., Chisty, E., Copley, A., 2016. Evolving strain partitioning in the Eastern Himalaya: the growth of the Shillong Plateau. Earth Planet. Sci. Lett. 433, 1–9. https://doi.org/10.1016/j.epsl.2015.10.017.

Nayak, G.K., Rao, V.K., Rambabu, H.V., Kayal, J.R., 2008. Pop-up tectonics of the Shillong Plateau in the great 1897 earthquake (Ms 8.7): insights from the gravity in conjunction with the recent seismological results. Tectonics 27, 1–8. https://doi.org/10.1029/2006TC002027.

Neal, R.M., 2003. Slice sampling. Ann. Stat. 31, 705–767. https://doi.org/10.1214/aos/1056562461.

Nikolaeva, K., Gerya, T.V., Marques, F.O., 2010. Subduction initiation at passive margins: numerical modeling. J. Geophys. Res. 115, B03406. https://doi.org/10.1029/2009JB006549.

Paul, J., Bürgmann, R., Gaur, V.K., Bilham, R., Larson, K.M., Ananda, M.B., Jade, S., Mukal, M., Anupama, T.S., Satyal, G., Kumar, D., 2001. The motion and active deformation of India. Geophys. Res. Lett. 28, 647–650. https://doi.org/10.1029/2000GL011832.

Perfettini, H., Avouac, J.-P., 2004. Stress transfer and strain rate variations during the seismic cycle. J. Geophys. Res., Solid Earth 109, 1–8. https://doi.org/10.1029/2003JB002917.

Priestley, K., Ho, T., Mitra, S., 2019. The crustal structure of the Himalaya: a synthesis. Geol. Soc. London, Spec. Publ. https://doi.org/10.1144/SP483-2018-127.

Rajendran, C.P., Rajendran, K., Duarah, B.P., Baruah, S., Earnest, A., 2004. Interpreting the style of faulting and paleoseismicity associated with the 1897 Shillong, northeast India, earthquake: implications for regional tectonism. Tectonics 23. https://doi.org/10.1029/2003TC001605, n/a–n/a.

Regenauer-Lieb, K., Yuen, D.A., Branlund, J., 2001. The initiation of subduction: criticality by addition of water? Science 80 (294), 578–580. https://doi.org/10.1126/science.1063891.

Rosenkranz, R., Schildgen, T., Wittmann, H., Spiegel, C., 2018. Coupling erosion and topographic development in the rainiest place on Earth: reconstructing the Shillong Plateau uplift history with in-situ cosmogenic 10Be. Earth Planet. Sci. Lett. 483, 39–51. https://doi.org/10.1016/j.epsl.2017.11.047.

Savage, J.C., 1983. A dislocation model of strain accumulation and release at a subduction zone. J. Geophys. Res. 88, 4984. https://doi.org/10.1029/JB088iB06p04984.

Schwanghart, W., Scherler, D., 2014. TopoToolbox 2 – MATLAB-based software for topographic analysis and modeling in Earth surface sciences. Earth Surf. Dyn. 2, 1–7. https://doi.org/10.5194/esurf-2-1-2014.

Steckler, M.S., Akhter, S.H., Seeber, L., 2008. Collision of the Ganges-Brahmaputra Delta with the Burma Arc: implications for earthquake hazard. Earth Planet. Sci. Lett. 273, 367–378. https://doi.org/10.1016/j.epsl.2008.07.009.

Steckler, M.S., Mondal, D.R., Akhter, S.H., Seeber, L., Feng, L., Gale, J., Hill, E.M., Howe, M., 2016. Locked and loading megathrust linked to active subduction beneath the Indo-Burman ranges. Nat. Geosci. 9, 615–618. https://doi.org/10.1038/ngeo2760.

Stern, R.J., 2004. Subduction initiation: spontaneous and induced. Earth Planet. Sci. Lett. 226, 275–292. https://doi.org/10.1016/j.epsl.2004.08.007.

Syracuse, E.M., van Keken, P.E., Abers, G.A., Suetsugu, D., Bina, C., Inoue, T., Wiens, D., Jellinek, M., 2010. The global range of subduction zone thermal models. Phys. Earth Planet. Inter. 183, 73–90. https://doi.org/10.1016/j.pepi.2010.02.004.

Talwani, M., Desa, M.A., Ismaiel, M., Sree Krishna, K., 2016. The tectonic origin of the Bay of Bengal and Bangladesh. J. Geophys. Res., Solid Earth 121, 4836–4851. https://doi.org/10.1002/2015JB012734.

Thompson, T. Ben, Plesch, A., Shaw, J.H., Meade, B.J., 2015. Rapid slip-deficit rates at the eastern margin of the Tibetan Plateau prior to the 2008 Mw7.9 Wenchuan earthquake. Geophys. Res. Lett., 1677–1684. https://doi.org/10.1002/2014GL062833. Abstract.

Vernant, P., Bilham, R., Szeliga, W., Drupka, D., Kalita, S., Bhattacharyya, a K., Gaur, V.K., Pelgay, P., Cattin, R., Berthet, T., 2014. Clockwise rotation of the Brahmaputra Valley relative to India: tectonic convergence in the eastern Himalaya, Naga Hills, and Shillong Plateau. J. Geophys. Res., Solid Earth 119, 6558–6571. https://doi.org/10.1002/2014JB011196.

Wang, X., Wei, S., Wang, Y., Maung Maung, P., Hubbard, J., Banerjee, P., et al., 2019. A 3-D shear wave velocity model for Myanmar region. J. Geophys. Res., Solid Earth 124, 504–526. https://doi.org/10.1029/2018JB016622.

Yin, A., Dubey, C.S., Webb, A.A.G., Kelty, T.K., Grove, M., Gehrels, G.E., Burgess, W.P., 2010. Geologic correlation of the Himalayan orogen and Indian craton: part 1. Structural geology, U-Pb zircon geochronology, and tectonic evolution of the Shillong Plateau and its neighboring regions in NE India. Bull. Geol. Soc. Am. 122, 336–359. https://doi.org/10.1130/B26460.1.